ChemPubSoc Europe

DOI: 10.1002/cphc.201700437

CHEMPHYSCHEM Articles

Special Issue

Computational Insights into the $CH_3Cl + OH$ Chemical Reaction Dynamics at the Air–Water Interface

Marilia T. C. Martins-Costa,[a] Josep M. Anglada,[b] and Manuel F. Ruiz-López*[a]

The reaction of methyl chloride with the hydroxyl radical OH is an important process in the troposphere. The kinetics of this reaction has been thoroughly studied in the gas phase, both experimentally and theoretically, but little is known about the effect of water on this reaction. In particular, investigating the reaction mechanism at the air–water interface is key in order to better understand the role of cloud water droplets and aerosols on the overall oxidation capacity of the troposphere. In this work, we have implemented a "rare event" approach combined to QM/MM (quantum mechanics and molecular mechanics) molecular dynamics simulations to investigate the dynamics of the H-abstraction reaction $CH_3Cl + OH \rightarrow CH_2Cl + H_2O$ at the air–water interface. For comparison, high-level ab initio calculations for the reaction mechanism in the gas phase are also reported and accurate kinetic constants at different temperatures are provided.

1. Introduction

Alkyl halides are an important class of halocarbon compounds in the troposphere. Methyl chloride, in particular, is the most abundant one and because of its long tropospheric lifetime (about 1.5 year), it supplies 0.5 ppb of chlorine into the stratosphere.[1] In this part of the atmosphere, CH_3Cl absorbs UV radiation and dissociates through photolysis to form Cl atoms, which play a key role on the ozone depletion process.[2]

The tropospheric budget of CH_3Cl is not yet completely understood however.[3] It is emitted into the atmosphere by both natural and anthropogenic sources.[4] Natural sources are the most important ones, with tropical forests being the largest contributor. Biomass burning, coastal salt marshes, industry and fuel combustion are also significant sources of CH_3Cl. Biogenic production involves an enzymatic process in which chloride methyltransferase catalyzes the S-adenosyl-L-methionine methylation of the chloride anion.[5] It has been suggested that spectroscopic signatures of CH_3Cl with simultaneous detection of O_2 or O_3 would be a strong evidence for life in extraterrestrial planets.[6] The main sink of CH_3Cl in the troposphere is reaction with OH, which produces water and the CH_2Cl radical [Eq. (1)]:[1]

$$CH_3Cl + OH \rightarrow CH_2Cl + H_2O \quad (1)$$

The experimental rate constant ranges between 3.65 and 4.46×10^{-14} $cm^3\,molecule^{-1}\,s^{-1}$ at 298 K.[3,7]

The atmospheric budget of volatile organic compounds such as CH_3Cl may be influenced by their interaction with cloud water droplets and aerosols, whose role on tropospheric chemistry begins to be recognized.[8] In fact, adsorption of gas-phase molecules on the air–water interface may be the cause of significant modifications of their reactivity. Recent computer simulations have provided key insights on this topic.[9] On one hand, it has been shown that interface solvation effects can be more intense than bulk solvation effects in water.[10] On the other hand, the air–water interface might influence the atmospheric budget of HO_x radicals significantly. For instance, we have shown that the OH formation rate from ozone photolysis is accelerated at the air–water interface by as much as 3–4 orders of magnitude compared to the same process in the gas phase.[11] The heterogeneous chemistry occurring at the air–water interface of water droplets in the troposphere is therefore a highly relevant research topic that deserves further exploration.

Some experiments on CH_3Cl at the air–water interface have been reported[12] as well as some theoretical works using classical molecular dynamics simulations.[13] Previous studies have focused on the preferred orientations of CH_3Cl and on the thermodynamics of the adsorption process. In the present work we have investigated, in a first step, the gas-phase $CH_3Cl + OH$ reaction and, in a second step, the hydration effects and the dynamics of the process at the air–water interface. We use high-level ab initio methods for the gas phase reaction and combined Quantum Mechanics and Molecular Mechanics (QM/MM)[14] molecular dynamics simulations for the reaction at the interface.

[a] Dr. M. T. C. Martins-Costa, Dr. M. F. Ruiz-López
SRSMC, University of Lorraine and CNRS
Boulevard des Aiguillettes, BP 70239, 54506, Vandoeuvre-lès-Nancy (France)
E-mail: Manuel.Ruiz@univ-lorraine.fr

[b] Dr. J. M. Anglada
Departament de Química Biològica i Modelització Molecular, IQAC, CSIC
c/ Jordi Girona 18, E-08034 Barcelona (Spain)

The ORCID identification number(s) for the author(s) of this article can be found under https://doi.org/10.1002/cphc.201700437.

An invited contribution to a Special Issue on Physical Chemistry in France

2. Computational Approach

The gas-phase reaction has been studied first. Geometry optimization and vibrational frequencies have been computed using Density Functional Theory based methods at the B3LYP level.[15] Two basis sets have been employed.[16] The 6-311+G(d,p) basis set has been used for comparison with simulations at the air–water interface (see below), but the geometries have been further refined using the 6-311+G(2df,2p), basis set in order to get more accurate data for the gas-phase kinetic parameters. At these levels of theory, we have also calculated the zero-point energies and the thermal contributions to enthalpy and Gibbs energy. In addition, intrinsic reaction coordinate (IRC) calculations[17] have been done to verify the connectivity between stationary points. Final energies were computed by performing single point energy calculations at the CCSD(T) level[18] using the aug-cc-pVTZ and aug-cc-pVQZ basis sets[19] and considering the extrapolation to the complete basis set (CBS) limit according to the scheme proposed by Helgaker et al.[20] These calculations have been carried out on B3LYP optimized geometries. Rate constants have been computed using variational (VTST) transition state theory[21] and the tunneling effects have been incorporated through the small curvature approach. Calculations have been done using the programs ORCA[22] and Gaussian[23] for the quantum chemical calculations, and Polyrate[24] for the kinetic study.

Calculations at the air–water interface have been carried out using QM/MM Molecular Dynamics (MD) simulations in the NVT ensemble at $T=298$ K with a Nosé-Hoover thermostat.[25] We assume a simulation box containing the reactant species (CH_3Cl, OH) and 499 water molecules described by the classical TIP3P force-field.[26] The box size is (in Å) $24.689\times24.689\times130$ and we use periodic boundary conditions along the X and Y directions. The reactant system CH_3Cl+OH is described at the B3LYP level with the 6-311+G(d,p) basis set. Note that the basis set used in our previous work[9] for methyl chloride alone was slightly different, 6-311+G(d). The time step is 0.25 fs. All the simulations have been done using the Gaussian program[23] for the QM calculations, Tinker 4.2[27] for the MD simulations and the interface developed by us.[28]

Several simulations have been done. In each case, the system has been conveniently equilibrated before the production run. In the first simulation (S1), the dynamics of CH_3Cl at the interface is analyzed through an unconstrained 300 ps trajectory carried out in our previous work.[9] In the second simulation (S2), we look at the dynamics of the transition structure (TS) for the CH_3Cl+OH reaction at the interface. In this case, we constrain the reaction coordinate (R_C) to its value in the gas-phase calculation. Our results for the energetics at the interface (see below) show that this is a suitable approximation for reaction (1). We use the approximated expression $R_C=d_{CH}-d_{OH}$, where d_{CH} and d_{OH} correspond to the breaking C–H and forming O–H bond distances, respectively. The trajectory was run for 155 ps. Finally, in the third simulation, we run a set of unconstrained trajectories starting from different configurations of S2. We integrate the equations of motion forward and backward in time (along 2.5 ps in each case) in order to reach either the reactants or the products. These two half trajectories are then linked together to finally get a set of trajectories 5 ps in length (S3) that reach the transition structure but can be reactive or non-reactive depending on the connected structures. They thus provide dynamical information on the chemical process according to the principles of the rare event approach (REA) theory[29] that we implemented in the framework of the QM/MM methodology.[30] For the reactive trajectories, we have recalculated the potential energy through single point energy calculations at CCSD(T)/aug-cc-pVTZ level of theory for a set of QM/MM MD snapshots, as explained below.

3. Results and Discussion

3.1. Gas-Phase Reaction

The gas-phase reaction has already been theoretically studied in the literature.[31] We report here further calculations for the sake of comparison with the process at the air–water interface. Our results compare, in general trends, with the previously published data. Nevertheless, since our computational level is slightly higher than those previously employed, we will briefly discuss the obtained results and compare them with previous studies, as it can be useful for updating the parameters used in current atmospheric models.

We have collected in Table 1 the relative energies for the CH_3Cl+OH reaction, and in Figure 1 the geometry of the relevant structures. Table 2 contains the results of the kinetic study. In this section we will only comment the values at the highest level of theory CCSD(T)/CBS//B3LYP/6-311+G(2df,2p), although Figure 1 and Table 1 contains also results at the lower level CCSD(T)/aug-cc-pVTZ//B3LYP/6-311+G(d,p) for comparison with calculations at the air–water interface below.

As in many atmospheric reactions, reaction (1) begins with the formation of the pre-reactive complex CR. In this complex, the two moieties (CH_3Cl and OH) are held together by a hydrogen bond, which is formed between the chlorine atom and the hydrogen atom of the hydroxyl radical. From this pre-reac-

Table 1. Relative energies, energies+ZPE, enthalpies and Gibbs free energies at 298 K (in kcal mol^{-1}) computed for the $CH_3Cl+OH\rightarrow CH_2Cl+H_2O$ reaction. See the corresponding structures in Figure 1.

Compound	ΔE	Δ(E+ZPE)	ΔH	ΔG
CH_3Cl+OH	0.00	0.00	0.00	0.00
CR[a]	−3.70	−2.61	−2.65	3.06
CR[b]	−3.43	−2.31	−2.39	3.42
TS[a]	4.74	3.56	2.76	10.67
TS[b]	4.47	3.34	2.55	10.25
CP[a]	−18.88	−18.86	−18.22	−14.29
CP[b]	−20.37	−20.37	−19.72	−15.75
CH_2Cl+H_2O[a]	−16.81	−18.18	−17.58	−19.04
CH_2Cl+H_2O[b]	−18.73	−20.05	−19.47	−20.86

[a] Electronic energies are computed at CCSD(T)/aug-cc-pVTZ//B3LYP/6-311+G(d,p) level. ZPE, enthalpic, and entropic corrections are computed at B3LYP/6-311+G(d,p) level. [b] Electronic energies are computed at the CCSD(T)/CBS//B3LYP/6-311+G(2df,2p) level. ZPE, enthalpic and entropic corrections are computed at the B3LYP/6-311+G(2df,2p) level.

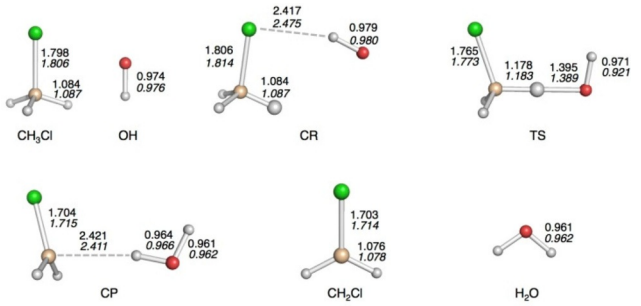

Figure 1. Optimized geometries of the relevant species for reaction (1) at the B3LYP/6-311+G(2df,2p) level. Some interatomic distances at this level are indicated with normal characters. Corresponding values for B3LYP/6-311+G(d,p) optimized structures are shown in italics. CR and CP correspond to the pre-reactive and post-reactive intermolecular complexes, respectively. Values in Å.

Table 2. Calculated values of the equilibrium constant (K_{eq} in $cm^3\,molecule^{-1}$), tunneling parameter (κ), unimolecular rate constant (k_2 in s^{-1}), and global rate constant (k in $cm^3\,molecule^{-1}\,s^{-1}$) for the $CH_3Cl+OH \rightarrow CH_2Cl+H_2O$ reaction.

T [K]	K_{eq}	κ	k_2	k
225	1.12×10^{-21}	4.02	1.81×10^{6}	8.14×10^{-15}
230	1.01×10^{-21}	3.77	2.39×10^{6}	9.10×10^{-15}
240	8.39×10^{-22}	3.37	4.01×10^{6}	1.13×10^{-14}
250	7.08×10^{-22}	3.04	6.45×10^{6}	1.39×10^{-14}
260	6.08×10^{-22}	2.77	9.99×10^{6}	1.68×10^{-14}
270	5.29×10^{-22}	2.55	1.50×10^{7}	2.03×10^{-14}
275	4.96×10^{-22}	2.46	1.81×10^{7}	2.21×10^{-14}
280	4.66×10^{-22}	2.38	2.18×10^{7}	2.42×10^{-14}
290	4.16×10^{-22}	2.23	3.09×10^{7}	2.86×10^{-14}
298	3.82×10^{-22}	2.13	4.01×10^{7}	3.26×10^{-14}
300	3.74×10^{-22}	2.10	4.27×10^{7}	3.36×10^{-14}
310	3.40×10^{-22}	1.99	5.79×10^{7}	3.91×10^{-14}
325	2.99×10^{-22}	1.85	8.81×10^{7}	4.87×10^{-14}

tive complex, the reaction proceeds to the transition state TS, which lies 3.34 kcal mol^{-1} above the energy of the reactants, then to the CP post-reactive complex before products are formed. Figure 1 shows that at the transition state, the OH moiety has a *syn*-periplanar configuration with the C–Cl bond. It displays a reactant-like structure,[31b] with the breaking C–H bond being significantly shorter that the forming O–H bond (d_{CH}-$d_{OH} \approx -0.2$ Å). Note that we have carried out an extensive search in order to ensure that a further transition state having a different configuration does not exist. Note also that our computed reaction enthalpy (−19.47 kcal mol^{-1}) is in excellent agreement with the value reported by Louis and co-workers[31a] (−19.48 kcal mol^{-1}).

According to the mechanism discussed for the CH_3Cl+OH reaction, the kinetic model can be written as displayed in Equation (2):

$$CH_3Cl + OH \underset{k_{-1}}{\overset{k_1}{\rightleftharpoons}} CH_3Cl\cdots OH \xrightarrow{k_2} CH_2Cl + H_2O \qquad (2)$$

so that the global rate constant k has been calculated following Equation (3):

$$k = \frac{k_1}{k_{-1}}k_2 = K_{eq}k_2 \qquad (3)$$

K_{eq} is the equilibrium constant for the pre-reactive complex, and has been calculated according to [Eq. (4)]:

$$K_{eq} = \frac{Q_{CH3Cl\cdots OH}}{Q_{CH3Cl}\,Q_{OH}} e^{-\frac{(E_{CR}-E_R)}{RT}} \qquad (4)$$

whereas for k_2 we have used the canonical variational transition state theory [Eq. (5)]:[21]

$$k_2 = \kappa\frac{k_b T}{h}\frac{Q_{GT}(s^*)}{Q_{CR}} e^{-\frac{V(s^*)}{k_b T}} \qquad (5)$$

Here, s^* is the free energy maximum along the reaction path at temperature T, $V(s^*)$ the corresponding potential energy, Q_{CR} is the partition function of the pre-reactive complex, $Q_{GT}(s^*)$ is the generalized transition state partition function, and κ is the tunneling parameter, which has been computed with the small curvature approach. Table 2 shows that our computed rate constant ranges between 8.14×10^{-15} $cm^3\,molecule^{-1}\,s^{-1}$ at 225 K and 4.87×10^{-14} $cm^3\,molecule^{-1}\,s^{-1}$ at 325 K. At room temperature, the computed value is 3.26×10^{-14} $cm^3\,molecule^{-1}\,s^{-1}$, which is in excellent agreement with the experimental values[3,7] ($3.65–4.46\times10^{-14}$ $cm^3\,molecule^{-1}\,s^{-1}$). Figure 2 displays the fitted Arrhenius equation in the temperature range 200–400 K, $k = 2.57\times10^{-12}\exp(-1303/T[K])$ in $cm^3\,molecule^{-1}\,s^{-1}$, where it is compared

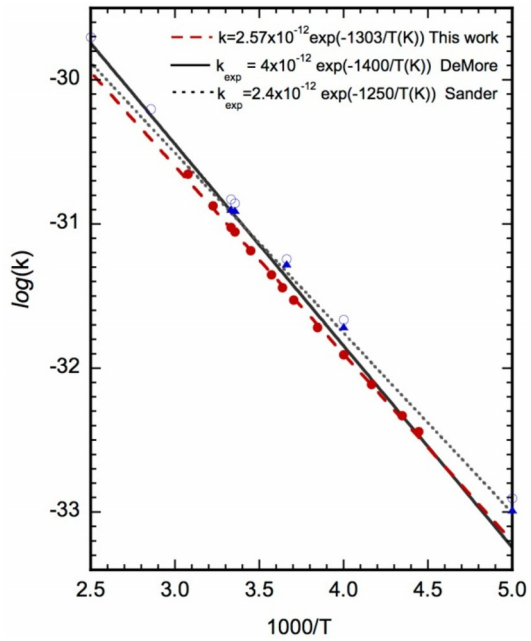

Figure 2. Comparison of the calculated Arrhenius equation in this work (dashed line) with experimental data reported by Sander et al[32] (dotted line) and by DeMore et al[33] (plain line); see also ref. [3]. The symbols correspond to ab initio calculations for the rate constant at different temperatures in this work (full circles), reported by Tzima et al[31b] (open circles) and by Dehestani et al[31d] (full triangles). Units of k are $cm^3\,molecule^{-1}\,s^{-1}$, and T is given in Kelvin.

with some experimental and theoretical values in the literature. As shown, the agreement with experiment is very good in the whole temperature range: at high temperature, the agreement is better with the more recent parameters reported by Sander et al.[32], whereas at low temperature, it fits better former parameters reported by DeMore et al.[33] Differences between the experimental Arrhenius equations could be attributed to the different methods used to obtain them, which combine relative and absolute measurements of kinetic data reported by several authors in the fitting procedure (for further details see the original references).

3.2. CH_3Cl Reactant Dynamics at the Air–Water Interface

Part of these results were already reported in ref. [9] and therefore we only make a summary here. First, the calculations show that CH_3Cl interacts weakly with the interface, as shown by the absence of noticeable features in the solute-solvent radial distribution functions.[9] In fact, CH_3Cl desorbs from the interface after about 220 ps in our simulation. When adsorbed at the interface, the center of mass of the molecule remains close to the formal interface, fluctuating between the water and the gas-phase layers. Its average position is approximately $Z=+0.4$ Å ($\sigma=1.5$ Å); $Z=0$ corresponds to the formal interface and the positive sign of Z corresponds to the gas-phase layer. Despite the weak strength of the CH_3Cl-water interaction, the rotational dynamics of the adsorbed system is modified so that some specific orientations are slightly favored, namely those in which the C–Cl bond is either parallel to the interface or pointing towards the air layer (Figure 3). The calculation of

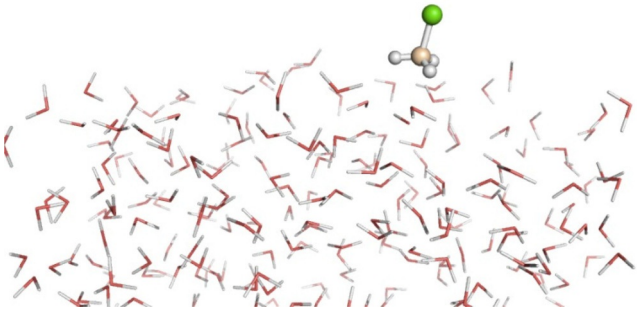

Figure 3. Snapshot of the QM/MM simulation S1 showing CH_3Cl at the air–water interface with the methyl group pointing typically towards the water layer.

the rotational autocorrelation function (using a second-order Legendre polynomial)[9] is satisfactorily fitted by a single exponential term and leads to a decay time of 0.36 ps, confirming the lack of long-time correlation. These findings support the view of CH_3Cl adsorbed at the air–water interface as a disordered system and are consistent with previous studies.[12,13] On one hand, vibrational sum frequency generation experiments[12] could not detect CH_3Cl at the interface, suggesting a low interface affinity of the molecule. On the other hand, classical MD simulations reported a short residence lifetime, estimated to 140 ps,[13c] and led to comparable conclusions concerning the relative orientation of the C–Cl bond with respect to the interface.[13a,b]

At the interface, the electronic properties of CH_3Cl change, both on average and in terms of time fluctuation amplitudes; in the following we consider the calculated averages using data from the 300 ps simulation when the system is close (adsorbed) or far (desorbed, gas phase) from the formal interface. The average dipole moment changes from 2.1 D (desorbed) to 2.5 D (adsorbed) while the average HOMO energy changes very slightly, from −0.302 au to −0.303 au in the same conditions, respectively. But the most important interface effect concerns the fluctuation of the properties, which is a key characteristic of solvation at liquid interfaces.[11] This is illustrated here with the HOMO energy in Figure 4, which clearly reveals that although the average property is not much changed, the distribution displays a completely different shape, quite narrow in the gas phase, very wide at the interface. Obviously, this effect is expected to influence the chemical reactivity of the molecule, despite its weak affinity for the air–water interface.

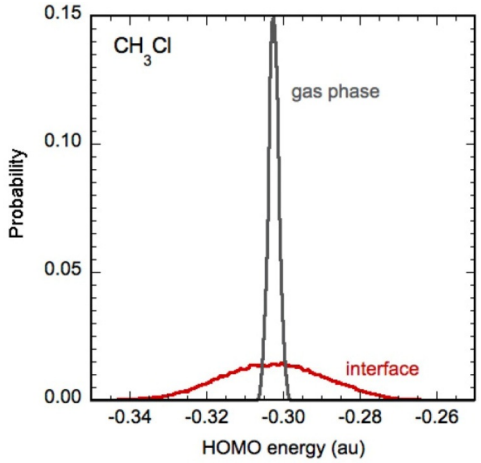

Figure 4. Normalized probability distribution of the HOMO energy of CH_3Cl in gas phase and at the air–water interface obtained in the QM/MM MD simulation.

3.3. Equilibrium Dynamics of the Transition Structure

We now examine the dynamics of the transition structure (TS) at the interface. The TS is constrained for a value of the reaction coordinate $R_C=-0.2$ Å, corresponding to the B3LYP/6-311+G(d,p) optimized structure in the isolated system. The first important result in simulation S2, is that the TS displays a certain interface affinity. It remains at the interface and no desorption or bulk accommodation processes have been observed at the time scale of the simulation. The average position of the center of mass of the TS lies roughly at $Z=+0.1$ Å ($\sigma=1.3$ Å), that is, basically on the formal interface plane. Indeed, the TS interacts more strongly with the solvent than the reactant methyl chloride because the OH subunit is involved in several hydrogen-bonds with water molecules. A typical snapshot is shown in Figure 5. In this Figure, we see the formation of two hydrogen bonds in which the TS is the H-ac-

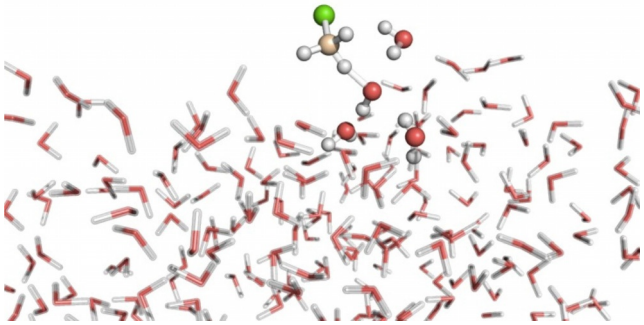

Figure 5. Snapshot of the TS at the air–water interface in the QM/MM simulation S2. The OH moiety of the TS forms hydrogen bonds with the three water molecules represented by balls and sticks.

ceptor, and one in which it is the H-donor. On average, the number of hydrogen-bonds along the simulation is 1.8 for $O_{TS}\cdots H_w$ bonds, and 1.0 for $H_{TS}\cdots O_w$ bonds.

We have already mentioned that the TS exhibits a reactant like structure on the basis of the breaking and forming bond distances. To further characterize this property at the interface, we have calculated the corresponding bond orders. For C–H, the average value in simulation S2 amounts 0.641, to be compared with the value 0.929 for the reactant CH_3Cl. For O–H, the average value in the TS simulation is 0.254, to be compared with the value 0.772 in the product water. Based on these values, it can be deduced that at the TS, the chemical bonds directly involved in the process have been modified by about 30–35% with respect to the total change required to reach the final values.

3.4. Reactive Trajectories

A total number of 398 initial configurations for the TS were considered and in each case a trajectory of 2.5 ps was launched for positive time, then for negative time (i.e. a total number of 796 trajectories were carried out for a total simulation time slightly smaller than 2 ns). From the full 398 trajectories, 117 (29%) were reactive, joining reactants to products, 262 (66%) were non- reactive trajectories linking products to products, and only a smaller fraction (5%) were non-reactive linking reactants to reactants. Note that in some reactive trajectories, after separation of the products, the quantum chemical calculation did not converge and the simulation stopped before completion. For simplicity, these incomplete reactive trajectories have not been considered for the calculation of the averages below, which has been done using the 98 complete reactive trajectories. Note also that we have arbitrarily reorganized the reactive trajectories so that in all cases negative time ($t<0$) corresponds to the reactant side while positive time ($t>0$) corresponds to the products side; the starting TS configuration designates $t=0$. Figure 6 displays a series of snapshots for one of the reactive trajectories at specific times before and after activation to the TS. In this case, the reactant CH_3Cl is initially in the air layer. A more detailed analysis of the reactants, TS and products distribution with respect to the formal interface plane is presented below.

Figure 7 shows the evolution of the reaction coordinate along the set of the 98 complete reactive trajectories. As shown, the fate of the system (reactants or products) is in general established quickly upon releasing the R_C constraint in the TS at $t=0$ in the REA simulations. Indeed, recrossings of the activation barrier in the simulations occur essentially at very short-times (below 20 fs) and only one trajectory (clearly seen in the Figure) exhibited a long time recrossing (at about 450 fs).

Nevertheless, an analysis of the time scale for the chemical reaction events can hardly be derived from the curves using the reaction coordinate alone because of the difficulty to unambiguously identify the reactants and products species using a simple geometrical parameter. To this end, it is far more useful to look at the time evolution of the electronic properties in the system. We have selected here the net atomic charge on the oxygen atom (calculated using the Natural Orbital Analysis), which as shown hereafter significantly changes along the reaction coordinate. However, similar conclusions can be

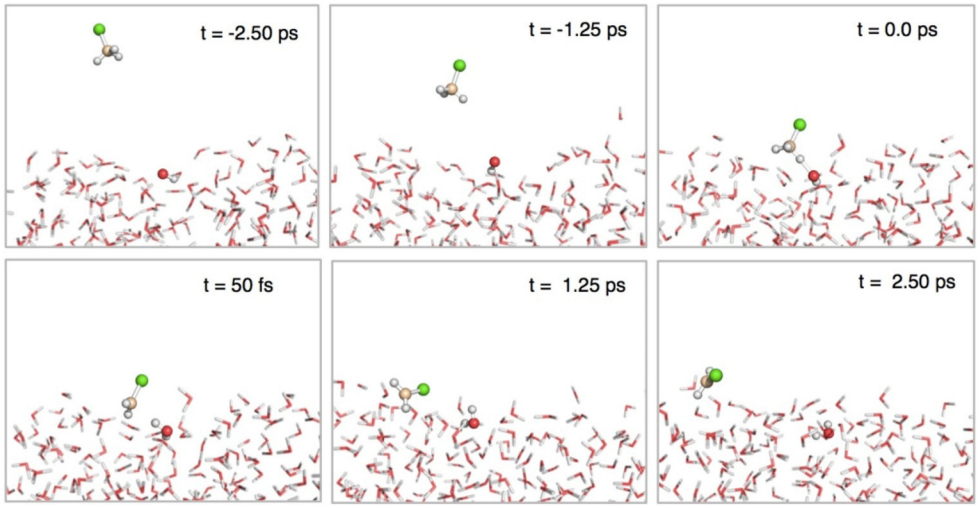

Figure 6. Example of reactive trajectory in the S3 simulations using the REA methodology.

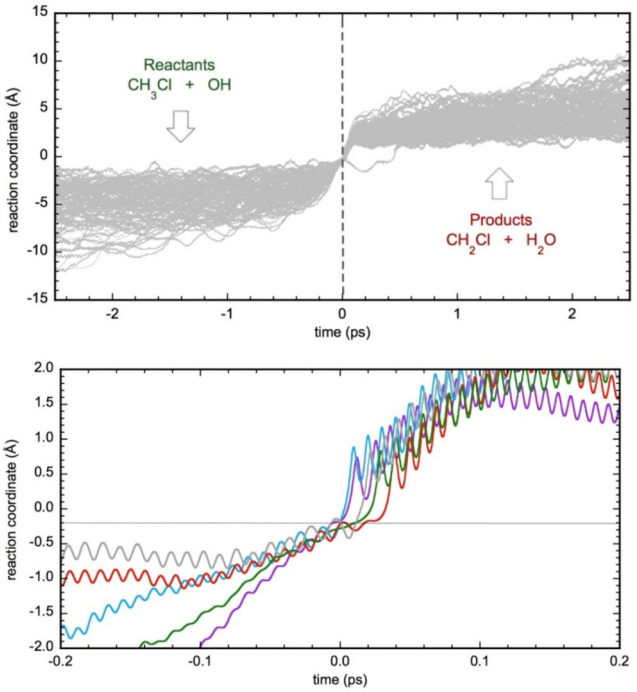

Figure 7. Time evolution of the reaction coordinate R_c for the calculated reactive trajectories. The origin of time ($t=0$) is arbitrarily chosen at the transition structure, that is, at the initial configuration in the REA formalism. The bottom Figure shows the curves around the TS at $t=0$ ($R_c=-0.2$ Å) in more detail for a particular subset of 5 trajectories.

reached using the net charge of the transferred hydrogen atom, or even the bond indexes of the chemical bonds being broken or created. Figure 8 shows the instantaneous value of the net charge on the O atom along the 98 reactive trajectories. The charge varies on average from −0.50 au in the reactants (OH radical) to −1.02 au in the products (water molecule) and amounts 0.74 au at the TS (considering the reactive trajectories only). The Figure shows that in the reactant part, some strong fluctuations of the oxygen charge occur in some trajectories, corresponding to situations in which the OH radical interacts with the H atoms of CH_3Cl and the O net atomic charge increases in absolute value. The average O charge has been fitted here by a 5-parameter (non-symmetric) generalized logistic function having the form [Eq. (6)]:

$$q(t) = A + \frac{B-A}{\left(1+ve^{-C(t-t_0)}\right)^{1/v}} \qquad (6)$$

The fit has been made using data in the range $t=\pm0.5$ ps. The corresponding curve and its first and third derivatives are shown in Figure 9. The different parameters have the following

Figure 8. Net atomic charge on the O atom along the reactive trajectories for the process $CH_3Cl+OH\rightarrow CH_2Cl+H_2O$.

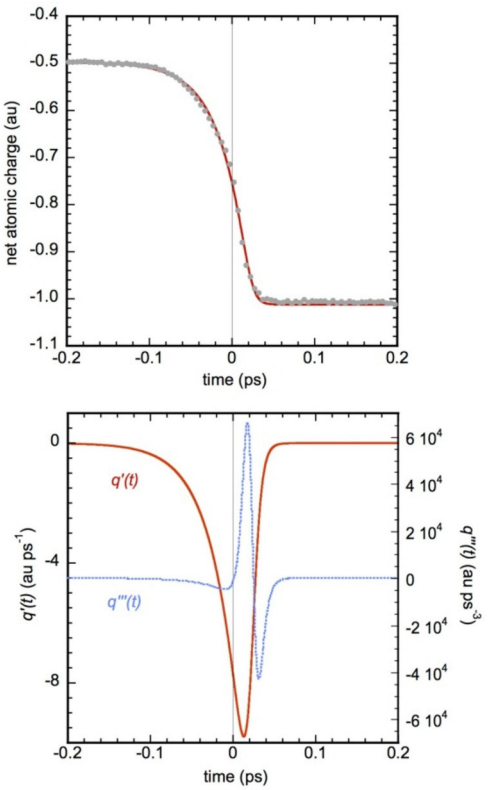

Figure 9. Top: average net atomic charge on the O atom (full circles) and fitted generalized logistic function (plain line) along the reactive trajectories for the process $CH_3Cl+OH\rightarrow CH_2Cl+H_2O$. Bottom: first and third derivatives of the fitted generalized logistic function.

physical meaning: A and B are the asymptotes at $t=-\infty$ and $t=+\infty$, respectively, that is, the initial and final O charges, C is a dimensionless growth rate, t_0 is the time of maximum growth, and $v>0$ is a dimensionless asymmetric parameter that affects near which asymptote maximum growth occurs. We obtain: $A=-0.498$ au, $B=-1.012$ au, $C=185.54$, $t_0=0.013$ ps and $v=6.062$ ($\chi^2=0.1$, $R^2=1.000$).

The first derivative of the net oxygen charge with respect to time, i. e. the charge transfer rate $q'(t)$, provides a suitable assessment for the advancement of the reaction. The reactant-like nature of the transition structure and the asymmetry of the process are clearly illustrated by this curve, which in addition provides an approximate time scale for the process. Thus,

one can consider that the reaction initiates at around $t=-120$ fs, when the O charge begins to increase. At this stage, about 1% of the total charge transfer has been done, and the average value of the reaction coordinate is $R_C=-1.74$ Å, corresponding to the formation of an intermolecular complex with a C–H···OH distance of roughly 2.8 Å. From then, the charge transfer and the charge transfer rate regularly rise until reaching the TS at $t=0$ ($R_C=-0.2$ Å). During this first part of the reaction, slightly less than 50% of the charge transfer has been accomplished. The transfer rate reaches a maximum (in absolute value) at $t_0=+13$ fs, where it amounts -9.79 au ps^{-1}; at this point $R_C=+0.30$ Å (the breaking CH bond distance is now longer than the forming OH bond distance) and 72% of the total charge has already been transferred. For the next 50 fs, the rate abruptly decreases to zero so that the charge transfer is virtually completed at $t=60$ fs, where $R_C=1.48$ Å corresponds to the formation of a CP type complex. The much faster variation of the charge transfer rate after activation to the TS ($0<t<60$ fs) is clearly illustrated by the huge values of the extrema in the $q'''(t)$ curve, shown in the bottom panel of Figure 9. To sum up, the total time necessary for the achievement of the reaction is estimated to 180 fs, and it is characterized by two different phases: a first stage of 130 fs during which one observes a progressive and regular increase of the charge transfer and transfer rate, and a second one of 50 fs during which a sharp decrease of the rate takes place.

An important aspect of chemical processes at the air–water interface needs now to be considered, namely how the reactants, transition structures and products distribute across the interface. In principle, one can expect some species to prefer the water layer while others might prefer the air layer, or even be unstable at the interface. Transition State Theory assumes solute-solvent equilibrium and strictly speaking, this requirement cannot be in general fulfilled for interfacial processes because the reaction time scale (180 fs in our case) is too short for the system to equilibrate through diffusion with regard to its relative position from the formal interface. In other words, the coordinate Z must be taken into account as a parameter that potentially can be responsible for non-equilibrium solvation effects on the reaction rate. Figure 10 provides the relevant distributions for the studied reaction and shows that the largest probability lies in the same region for all the species, slightly inside the water layer with Z around 8 Å and 10 Å for the O and C atoms, respectively. Nevertheless, there is a non-negligible probability to find the C atom in the air layer, especially for reactants, which is not surprising after considering the small residence time of methyl chloride described above. Indeed, in some trajectories CH_3Cl lies clearly in the air layer at the initial reaction time $t=-2.5$ ps, as in the case of the trajectory illustrated in Figure 6. On average, the diffusion across the interface around the reactive events is estimated to be rather small. To quantify this property, we can look at the mean-square displacement, which is related to the Einstein expression for the self-diffusion coefficient [Eq. (7)]:

$$6Dt = \lim_{t\to\infty} < \left(\boldsymbol{r}\left(t' + t\right) - \boldsymbol{r}(t')\right)^2 > \qquad (7)$$

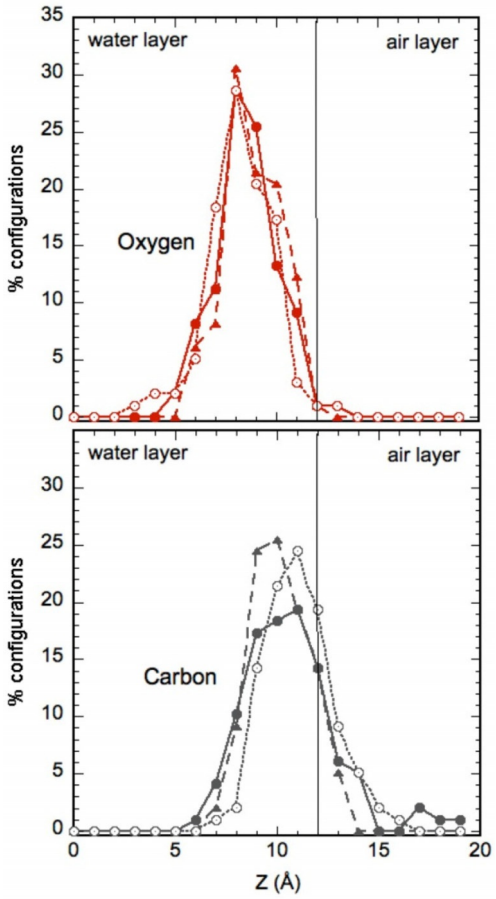

Figure 10. Distribution of reactants (full circles), transition structure (triangles) and products (circles) across to the air–water interface. The distributions of reactants and products are taken at 2.5 ps before and after reaching the TS, respectively, in the 98 complete reactive trajectories.

Here we focus on the Z-displacement with respect to the initial position at $t=0$ over the 98 trajectories [Eq. (8)]

$$\xi^2 = < (Z(t) - Z(0))^2 > \qquad (8)$$

and estimate its value at the end of the trajectory on the reactant or product sides after $t=\pm 2.5$ ps (using C and O atom coordinates). We obtain 4.4 Å^2, 3.9 Å^2, 1.8 Å^2 and 1.6 Å^2, for CH_3Cl, CH_2Cl, OH and H_2O, respectively. The TIP3P self-diffusion coefficient of H_2O molecules in bulk water at 298 K is 5.65×10^{-9} m^2 s^{-1},[34] which leads to a mean-square displacement in one dimension of 2.8 Å^2 for $t=2.5$ ps that is significantly larger than the calculated value of ξ^2 for the water product formed in the reaction at the interface. The diffusion of the species across the interface is an interesting issue that deserves further attention but our calculations, despite the limited number of trajectories considered, provide some qualitative trends. They suggest a slow diffusion of the species across the interface compared to the bulk, especially for the hydrophilic ones.

Finally, let us consider the energetics of the reaction at the interface. The calculation of free energy surfaces at the QM/MM level is computationally expensive and has not been done here. Rather, we look at the average potential energies along

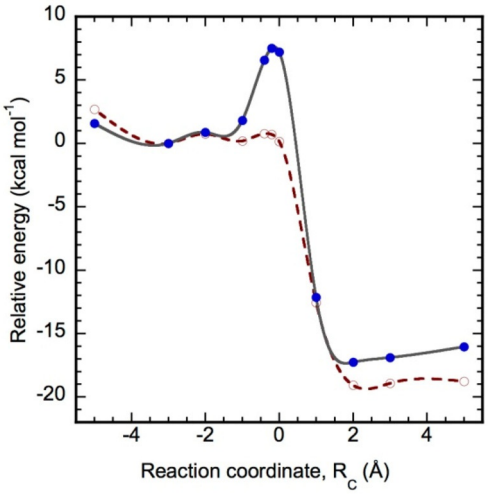

Figure 11. Average potential energy profiles of the reaction at the air–water interface. B3LYP/6-311+G(d,p) calculations (open circles, dashed line) and corrected profile with CCSD(T)/aug-cc-pVTZ calculations (full circles, plain line). The curves correspond to a cubic spline fitting of the calculated points.

the reaction coordinate and compare them to the potential energy calculated for the isolated species. The aim is to get insights on the role of QM/MM solute-solvent interaction on the reaction energy profile. Figure 11 displays the average potential energy $< V(R_C) >$ calculated at the B3LYP and CCSD(T)-corrected levels [Eq. (9)]:

$$< V(R_C) > = < E_{QM} > + < E_{QM/MM} > \quad (9)$$

Here, the averages are calculated using the reactive trajectories, E_{QM} represents the potential energy of the quantum system (the reactants) and $E_{QM/MM}$ represents the solute-solvent interaction energy, which contains electrostatic and non-electrostatic interactions. The CCSD(T)-corrected curve is obtained using the expression [Eq. (10)]:

$$< V_{CCSD(T)} >_a \approx < V_{B3LYP} >_a + < V_{CCSD(T)} - V_{B3LYP} >_b \quad (8)$$

where the averages are calculated using the whole set of recorded snapshots (*a*) or a subset of 10% snapshots (*b*) for a specific value of the reaction coordinate ± 0.05 Å.

The B3LYP and CCSD(T)-corrected curves have a similar shape as the gas-phase energy profile, with the presence of minima before and after the TS (note however the shallow double well obtained in the reactants side, which is not necessarily physical and could be due to limited statistical accuracy). At the CCSD(T) level, the activation energy is 7.6 kcal mol^{-1}, a little smaller than the activation energy in gas phase at the same level, 8.4 kcal mol^{-1}, while the reaction energy (or more precisely, the difference between the reactant and product complexes) is -17.3 kcal mol^{-1}, slightly larger in absolute value than the gas-phase result, -15.2 kcal mol^{-1}. These results do not account for the water reorganization energy, ZPE, thermal contributions, etc, but they predict a small modification of the potential energy surface of the chemical system through the interaction with water. The effect would contribute to slightly favor the kinetics of the process and its exothermicity.

4. Conclusions

In this paper, we have reported theoretical results for the H-abstraction reaction $CH_3Cl + OH \rightarrow CH_2Cl + H_2O$, which is an important process in the troposphere. Accurate ab initio calculations in the gas phase have led to the Arrhenius equation $k = 2.57 \times 10^{-12}$ exp($-1303/T$[K]) in cm^3 molecule^{-1} s^{-1}, which is in excellent agreement with experimental data and also some previous theoretical studies. The main aim of our work was to analyze the dynamics of the process at the air–water interface. This has been done using combined QM/MM MD simulations and the rare event approach for sampling the region of the transition structure and obtaining a representative set of 398 trajectories of 5 ps each. The ratio between reactive and non-reactive trajectories is close to 30%, suggesting a significant dynamic solvation effect. We have shown that the process at the interface, like in the gas phase, is characterized by a reactant-like transition state and by the formation of pre-reactive and post-reactive complexes that are associated to minima in the potential energy surface of the system. Due to the high computational cost, we were not able to report free energy surfaces and therefore to make an estimation of the reaction kinetics and thermodynamics at the interface. However, the trends in the average potential energy suggest that the solute-solvent interactions should reduce slightly the activation energy and increase the exothermicity of the process. The reaction time has been estimated by means of the time evolution of the net atomic charge on the O atom. It leads to a reaction time of 180 fs divided into two parts and characterized by a progressive increase of the charge transfer rate (first 120 fs) followed a fast decrease of this rate (last 60 fs). The computational approach implemented in this work paves the way to future studies of chemical reactions at aqueous interfaces, a topic that remains poorly understood despite its high relevance in environmental, atmospheric, and even biological chemistry.

Acknowledgements

The authors are grateful to the French CNRS and the Spanish CSIC organizations for funding a collaborative PICS project (PIC2015FR1). M.M.C. and M.F.R.L. are grateful to the French CINES (project lct2550) for providing computational resources. J.M.A. thanks the Spanish Secretaria de Estado de Investigación, Desarrollo e Innovación (CTQ2014-59768-P) and the Generalitat de Catalunya (Grant 2014SGR139) for financial support, and the Consorci de Serveis Universitaris de Catalunya (CSUC) for providing computational resources.

Conflict of interest

The authors declare no conflict of interest.

Keywords: atmospheric chemistry · methyl chloride · molecular dynamics simulations · reaction dynamics · water interfaces

[1] J. H. Seinfeld, S. N. Pandis, *Atmospheric Chemistry and Physics: From Air Pollution to Climate Change*, 2nd ed., Wiley, Hoboken, **2006**.
[2] S. A. Montzka in *Stratospheric Ozone Depletion and Climate Change* (Ed.: R. Muller), RSC Publishing, **2012**, pp 33 – 77.
[3] Y. Yoshida, Y. H. Wang, T. Zeng, R. Yantosca, *J. Geophys. Res. Atmos.* **2004**, *109*, D24309.
[4] a) M. Khalil, R. Moore, D. Harper, J. Lobert, D. Erickson, V. Koropalov, W. Sturges, W. Keene, *J. Geophys. Res. Atmos.* **1999**, *104*, 8333 – 8346; b) Y. Yokouchi, A. Takenaka, Y. Miyazaki, K. Kawamura, T. Hiura, *J. Geophys. Res. Biogeosci.* **2015**, *120*, 1142 – 1149.
[5] R. C. Rhew, L. Østergaard, E. S. Saltzman, M. F. Yanofsky, *Curr. Biol.* **2003**, *13*, 1809 – 1813.
[6] A. Segura, J. F. Kasting, V. Meadows, M. Cohen, J. Scalo, D. Crisp, R. A. Butler, G. Tinetti, *Astrobiology* **2005**, *5*, 706 – 725.
[7] NIST Chemical Kinetics Database, in http://kinetics.nist.gov/kinetics/index.jsp, *accessed March 2017*.
[8] a) A. R. Ravishankara, *Science* **1997**, *276*, 1058 – 1065; b) A. R. Ravishankara, C. A. Longfellow, *Phys. Chem. Chem. Phys.* **1999**, *1*, 5433 – 5441; c) A. Monod, P. Carlier, *Atmos. Environ.* **1999**, *33*, 4431 – 4446; d) J. D. Blando, B. J. Turpin, *Atmos. Environ.* **2000**, *34*, 1623 – 1632; e) D. J. Jacob, *Atmos. Environ.* **2000**, *34*, 2131 – 2159; f) J. P. Reid, R. M. Sayer, *Sci. Prog.* **2002**, *85*, 263 – 296; g) B. J. Finlayson-Pitts, *Phys. Chem. Chem. Phys.* **2009**, *11*, 7760 – 7779; h) C. E. Kolb, R. A. Cox, J. P. D. Abbatt, M. Ammann, E. J. Davis, D. J. Donaldson, B. C. Garrett, C. George, P. T. Griffiths, D. R. Hanson, M. Kulmala, G. McFiggans, U. Poschl, I. Riipinen, M. J. Rossi, Y. Rudich, P. E. Wagner, P. M. Winkler, D. R. Worsnop, C. D. O'Dowd, *Atmos. Chem. Phys.* **2010**, *10*, 10561 – 10605; i) H. Liang, Z. Chen, D. Huang, Y. Zhao, Z. Li, *Atmos. Chem. Phys.* **2013**, *13*, 11259 – 11276; j) H. Herrmann, T. Schaefer, A. Tilgner, S. A. Styler, C. Weller, M. Teich, T. Otto, *Chem. Rev.* **2015**, *115*, 4259 – 4334; k) C. George, M. Ammann, B. D'Anna, D. Donaldson, S. A. Nizkorodov, *Chem. Rev.* **2015**, *115*, 4218 – 4258.
[9] M. T. C. Martins-Costa, M. F. Ruiz-López, in *Quantum Modeling of Complex Molecular Systems* (Eds.: J.-L. Rivail, M. Ruiz-Lopez, X. Assfeld), Springer International Publishing, Cham, **2015**, pp. 303 – 324.
[10] a) M. T. C. Martins-Costa, J. M. Anglada, J. S. Francisco, M. Ruiz-Lopez, *Angew. Chem. Int. Ed.* **2012**, *51*, 5413 – 5417; *Angew. Chem.* **2012**, *124*, 5509 – 5513; b) M. T. C. Martins-Costa, J. M. Anglada, J. S. Francisco, M. F. Ruiz-Lopez, *J. Am. Chem. Soc.* **2012**, *134*, 11821 – 11827; c) M. T. C. Martins-Costa, F. F. Garcia-Prieto, M. F. Ruiz-Lopez, *Org. Biomol. Chem.* **2015**, *13*, 1673 – 1679; d) M. C. Martins-Costa, M. Ruiz-Lopez, *Theor. Chem. Acc.* **2015**, *134*, 17.
[11] J. M. Anglada, M. Martins-Costa, M. F. Ruiz-Lopez, J. S. Francisco, *Proc. Natl. Acad. Sci. USA* **2014**, *111*, 11618 – 11623.
[12] K. Harper, B. Minofar, M. R. Sierra-Hernandez, N. N. Casillas-Ituarte, M. Roeselova, H. C. Allen, *J. Phys. Chem. A* **2009**, *113*, 2015 – 2024.
[13] a) H. Pašalić, M. Roeselová, H. Lischka, *J. Phys. Chem. B* **2011**, *115*, 1807 – 1816; b) A. Habartová, K. T. Valsaraj, M. Roeselová, *J. Phys. Chem. A* **2013**, *117*, 9205 – 9215; c) A. Habartová, A. Obisesan, B. Minofar, M. Roeselová, *Theor. Chem. Acc.* **2014**, *133*, 1455.
[14] a) A. Warshel, M. Levitt, *J. Mol. Biol.* **1976**, *103*, 227 – 249; b) P. A. Bash, M. J. Field, M. Karplus, *J. Am. Chem. Soc.* **1987**, *109*, 8092 – 8094; c) I. Tuñón, M. T. C. Martins-Costa, C. Millot, M. F. Ruiz-Lopez, *Chem. Phys. Lett.* **1995**, *241*, 450 – 456.
[15] A. D. Becke, *J. Chem. Phys.* **1993**, *98*, 5648 – 5652.
[16] R. Krishnan, J. S. Binkley, R. Seeger, J. A. Pople, *J. Chem. Phys.* **1980**, *72*, 650 – 654.
[17] C. Gonzalez, H. B. Schlegel, *J. Phys. Chem.* **1990**, *94*, 5523 – 5527.
[18] a) J. Cizek, *Adv. Chem. Phys.* **1969**, *14*, 35; b) J. A. Pople, R. Krishnan, B. Schlegel, J. S. Binkley, *Int. J. Quantum Chem.* **1978**, *14*, 545; c) R. J. Bartlett, *J. phys. Chem.* **1989**, *93*, 1697.
[19] a) T. H. J. Dunning, *J. Chem. Phys.* **1989**, *90*, 1007 – 1023; b) R. A. Kendall, T. H. Dunning, R. J. Harrison, *J. Chem. Phys.* **1992**, *96*, 6796.
[20] K. L. Bak, J. Gauss, P. Jørgensen, J. Olsen, T. Helgaker, J. F. Stanton, *J. Chem. Phys.* **2001**, *114*, 6548 – 6556.
[21] D. G. G. Truhlar, *Acc. Chem. Res.* **1980**, *13*, 440 – 448.
[22] F. Neese, *WIREs Comput. Mol. Sci.* **2012**, *2*, 73 – 78.
[23] M. J. Frisch, G. W. Trucks, H. B. Schlegel, G. E. Scuseria, M. A. Robb, J. R. Cheeseman, G. Scalmani, V. Barone, B. Mennucci, G. A. Petersson, H. Nakatsuji, M. Caricato, X. Li, H. P. Hratchian, A. F. Izmaylov, J. Bloino, G. Zheng, J. L. Sonnenberg, M. Hada, M. Ehara, K. Toyota, R. Fukuda, J. Hasegawa, M. Ishida, T. Nakajima, Y. Honda, O. Kitao, H. Nakai, T. Vreven, J. A. Montgomery, Jr., J. E. Peralta, F. Ogliaro, M. J. Bearpark, J. Heyd, E. N. Brothers, K. N. Kudin, V. N. Staroverov, R. Kobayashi, J. Normand, K. Raghavachari, A. P. Rendell, J. C. Burant, S. S. Iyengar, J. Tomasi, M. Cossi, N. Rega, N. J. Millam, M. Klene, J. E. Knox, J. B. Cross, V. Bakken, C. Adamo, J. Jaramillo, R. Gomperts, R. E. Stratmann, O. Yazyev, A. J. Austin, R. Cammi, C. Pomelli, J. W. Ochterski, R. L. Martin, K. Morokuma, V. G. Zakrzewski, G. A. Voth, P. Salvador, J. J. Dannenberg, S. Dapprich, A. D. Daniels, Ö. Farkas, J. B. Foresman, J. V. Ortiz, J. Cioslowski, D. J. Fox, Gaussian, Inc., Wallingford, CT, USA, **2009**.
[24] D. H. Lu, T. N. Truong, V. S. Melissas, G. C. Lynch, Y.-P. Liu, B. C. Garrett, R. Steckler, A. D. Isaacson, S. N. Rai, G. C. Hancock, J. G. Lauderdale, T. Joseph, D. G. Truhlar, *Comput. Phys. Commun.* **1992**, *71*, 235 – 262.
[25] a) S. Nosé, *J. Chem. Phys.* **1984**, *81*, 511; b) W. G. Hoover, *Phys. Rev. A* **1985**, *31*, 1695.
[26] W. L. Jorgensen, J. Chandrashekar, J. D. Madura, W. R. Impey, M. L. Klein, *J. Chem. Phys.* **1983**, *79*, 926 – 935.
[27] J. W. Ponder, 4.2 ed., Washington University School of Medicine: Saint Louis, MO., **2004**.
[28] a) M. T. C. Martins-Costa, University of Lorraine—CNRS, **2014**; b) M. T. C. Martins-Costa, M. F. Ruiz-Lopez, *Chem. Phys.* **2007**, *332*, 341 – 347.
[29] a) J. B. Anderson, *J. Chem. Phys.* **1973**, *58*, 4684 – 4692; b) J. B. Anderson, *Adv. Chem. Phys.* **1995**, *91*, 381 – 431.
[30] a) M. Strnad, M. T. C. Martins-Costa, C. Millot, I. Tuñón, M. F. Ruiz-López, J. L. Rivail, *J. Chem. Phys.* **1997**, *106*, 3643; b) A. Soriano, E. Silla, I. Tuñón, M. F. Ruiz-López, *J. Am. Chem. Soc.* **2005**, *127*, 1946; c) S. Chalmet, W. Harb, M. F. Ruiz-López, *J. Phys. Chem. A* **2001**, *105*, 11574 – 11581.
[31] a) F. Louis, C. A. Gonzalez, R. E. Huie, M. J. Kurylo, *J. Phys. Chem. A* **2000**, *104*, 8773 – 8778; b) T. D. Tzima, D. K. Papayannis, V. S. Melissas, *Chem. Phys.* **2005**, *312*, 169 – 176; c) S. R. Sellevåg, G. Nyman, C. J. Nielsen, *J. Phys. Chem. A* **2006**, *110*, 141 – 152; d) M. Dehestani, F. Shojaie, *Int. J. Quantum Chem.* **2012**, *112*, 1307 – 1315.
[32] S. Sander, R. Friedl, D. Golden, M. Kurylo, R. Huie, V. Orkin, G. Moortgat, A. Ravishankara, C. Kolb, M. Molina, *NASA Jet Propulsion Lab., Pasadena, Calif* **2003**.
[33] W. DeMore, S. Sander, D. Golden, R. Hampson, M. Kurylo, C. Howard, A. Ravishankara, C. Kolb, M. Molina, *Pasadena, CA* **1997**.
[34] P. Mark, L. Nilsson, *J. Phys. Chem. A* **2001**, *105*, 9954 – 9960.

Manuscript received: April 23, 2017
Revised manuscript received: June 2, 2017
Accepted manuscript online: June 6, 2017
Version of record online: June 14, 2017